

The Use of Microwave Radar for Remote Detection of Gas Pipeline Leaks

By

N. Gopalsami, A. Dron, T. Elmer, and A. C. Raptis
Energy Technology Division
Argonne National Laboratory
Argonne, IL

and

V. D. Asanov, S. V. Kokhatski, and S. A. Mishin
AOZT Finn-Trade
St. Petersburg, Russia

Abstract:

This report describes the development of a microwave (MW) radar sensing and imaging system to remotely detect and locate gas leaks in natural gas pipelines. It contains theoretical and experimental results to show feasibility of the radar technique. The gas dynamics of the leak jet are modeled first to determine the plume geometry and the variation of gas concentration in air with distance from the leak source. From the turbulence-induced static and dynamic changes of index of refraction, the radar backscatter cross section of the plume is determined next. To verify the model predictions and to determine the detection sensitivity of gas leaks, a commercial X-band radar system was interfaced with a computer to enable data collection and specialized signal and image processing. The radar, calibrated with a corner cube, was tested on gas plumes (cold nitrogen for initial test and propane leak for long-range test). The radar cross sections of gas plumes, calculated from the test data, were in the general range of the model predictions. The results thus indicate the technical feasibility of the radar technique for remote and fast inspection of gas pipelines for leaks.

I Introduction

The U.S. natural gas infrastructure is large and expansive, covering the country over 2 million miles of transmission and distribution pipelines from bore wells to homes and industries. Also, the natural gas demand is projected to increase by 50% by the year

2020.¹ This coupled with the fact that most of the existing infrastructure is old and aging, raises a great concern for long-term gas reliability and infrastructure integrity. Leaks, for example, can develop in any part of the transmission and distribution lines due to pipe corrosion, third party damage, or failure of valves and joints. Because of the flammable nature of the gas, leaks can be deadly and disrupt service to thousands of customers. Remote and fast inspection tools are, therefore, of paramount importance for early detection and prevention of gas leaks.

Current leak detection systems are based on sniffing or drawing of air samples from inspection location. These point-sensing devices, although they may work well, are labor intensive and impractical for inspecting the vast network of pipes. The nature and scale of the problem calls for remote sensing techniques that can monitor the gas pipelines around the clock to image/locate minute leaks. Wave techniques using visible, infrared, ultraviolet, microwave, or millimeter wave bands of the electromagnetic spectrum offer potential for remote sensing. While these techniques are routinely used in satellite-based remote sensing and imaging of the Earth resources and weather forecasting, their application to chemical detection is still in their early stages.

This report describes a microwave radar method for remote and fast imaging of gas leaks. The underlying principle is the change in radar reflection, refraction, and scattering properties of leak plumes with respect to the surrounding air. The problem of radar detection of gas leaks from a point source is akin to meteorological targets in weather prediction — both deal with gas-phase media and the volume scattering from dielectric property changes. The source of radar returns in meteorological radars is the change of reflectivity, refraction, and scattering caused by storms, rain, cloud, atmospheric turbulence, and wind movement. Even in the absence of contrasting dielectric materials such as water and ice droplets in the atmosphere, the radars can detect clear-air turbulence and wind shear due to wave scattering caused by index of refraction inhomogeneities.²⁻³

The basis of microwave (MW) radar measurements lies in the radar equation:⁴⁻⁵

$$P_r = \frac{P_t G^2 \lambda^2 \sigma}{(4\pi)^3 R^4}, \quad (1)$$

where P_r is the received power, P_t the transmitter power, G the gain of the transmit/receive antenna, λ the wavelength, R the distance to the plume, and σ the radar cross section of the plume. The radar cross section of the gas plume depends on its complex dielectric constant denoted by $\epsilon = \epsilon' - j\epsilon''$, where the real part, ϵ' , is the relative permittivity (responsible for reflection and refraction ($n^2 = \epsilon'$)) and the imaginary part, ϵ'' , is the loss factor (responsible for absorption). It also depends on the scattering from the index of refraction fluctuation caused by the gas cloud. Other factors that can play a role in the radar return include wavelength, incident angle, and polarization diversity.

The purpose of this report is to provide a technical basis for radar measurements and to show its feasibility to remotely detect gas plumes. The end goal is to build a van-mounted or airborne microwave imaging radar to detect above- or below-ground pipe leaks. In what follows, the report describes (i) a model for calculating the radar cross section σ of leak plumes from a natural gas pipeline, (ii) the development of an X-band radar tailored for gas plume detection, and (iii) radar test results on gas plumes.

II Plume Model

The purpose of modeling is (a) to determine the feasible radar range of gas plume detection and (b) to fine tune the radar parameters for optimal detection. The pipeline is assumed to contain methane at a pressure of 50 kg/cm². Three classes of leaks are considered corresponding to 5.4, 17, and 54 mm holes in the pipe. The model has two parts: (a) gas dynamic model to determine the plume dispersion, methane concentration, and the corresponding index of refraction of methane-air mixture and (b) scattering model based on index of refraction inhomogeneities to estimate the radar cross section.

The leak jet emanating into the atmosphere from a small hole in a pressurized gas pipeline is turbulent in nature and takes the shape of a cone (Fig. 1). The character of the jet flow is described the forces of inertia, viscosity, and buoyancy; it is characterized by

three flow zones dominated by the inertial, intermediate, and buoyancy forces. The gas flow velocity in each flow zone is described by integral equations of motion, energy conservation, and plume spread.⁶

$$\frac{d}{dx} \int_0^{\delta/2} \rho u^2 \pi y dy = -g \int_0^{\delta/2} (\rho - \rho_a) \pi y dy, \quad (2)$$

$$\frac{d}{dx} \int_0^{\delta/2} u (\rho - \rho_a) \pi y = 0, \quad (3)$$

$$\delta = c \cdot x. \quad (4)$$

where ρ is the density of methane-air mixture, ρ_a the density of air, u the velocity of gas, g the acceleration due to gravity, δ the diameter of the jet, c a constant equal to 0.44, and (x,y) are the coordinate variables along the jet axis and lateral to the jet axis, respectively.

Assuming a gas pressure of 50 kg/cm² in the pipeline, the initial velocity of the leak flow is 739 m/s. Consider three leak sizes with leak holes of diameter 5.4 mm, 17 mm, and 54 mm. Based on Eq. (3), the plume size (diameter) with distance from the leak is given in Fig. 2(a); note that the plume size does not depend on the size of the leak hole. We can determine the flow velocities in each zone by introducing in Eqs. (2) and (3) a lateral flow profile given by Schlichting's formula:⁵

$$u(y) = \left[1 - \left(\frac{2y}{\delta} \right)^{1.5} \right]^2 u_m \quad (5)$$

where u_m is the velocity along the jet axis and $u(y)$ is the velocity along the lateral axis. Figure 2(b) gives the flow velocity changes along the jet axis as a function of leak distance.

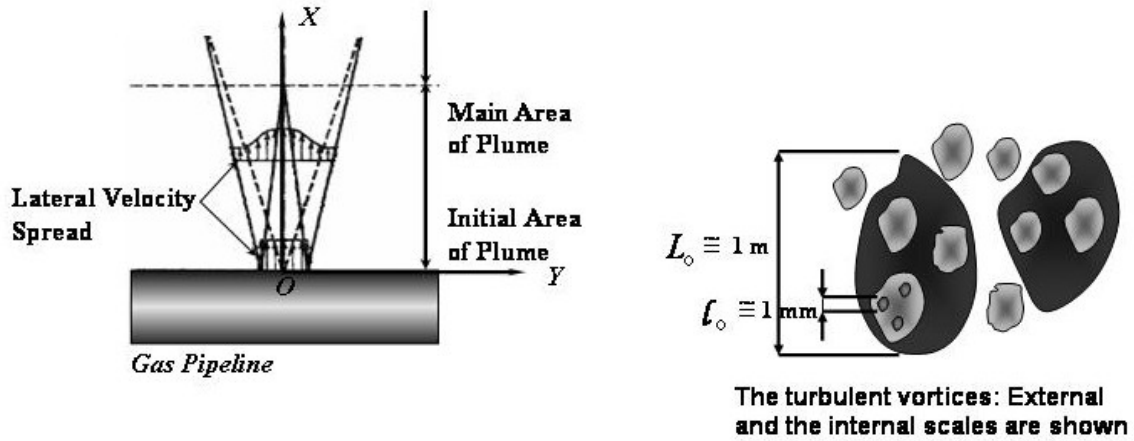


Fig. 1. Plume geometry with turbulent vortices.

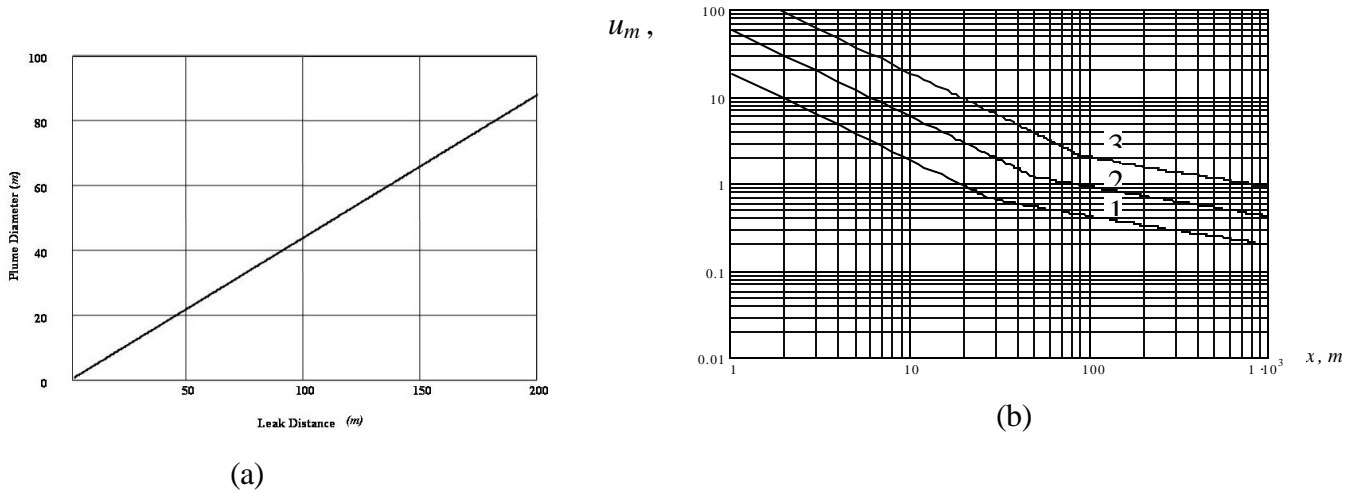


Fig. 2. (a) Plume diameter and (b) flow velocity vs. leak distance.

Substituting $\rho = \rho_a$ at $y = \delta/2$ in Eq. (2),

$$\rho_m - \rho_a = \frac{2B}{A_3 u_m \delta^2}, \quad (6)$$

and the normalized density change in the jet

$$\Delta \bar{\rho}_m = \frac{\rho_m - \rho_a}{\rho_0 - \rho_a} = \frac{u_0 d_0^2}{2 A_3 c^2 u_m x^2}, \quad (7)$$

where ρ_m is the density along the jet axis, ρ_a the density of air, d_0 the diameter of the leak hole, and B , A_3 and c are constants.

The change in the mass concentration due to flow changes in the three zones is shown in Fig. 3 for three holes of diameter 5.4 mm, 17 mm, and 54 mm. For example, the plume diameter is 44 m and the methane concentration is 100 ppm at a distance of 100 m from a 5.4 mm leak.

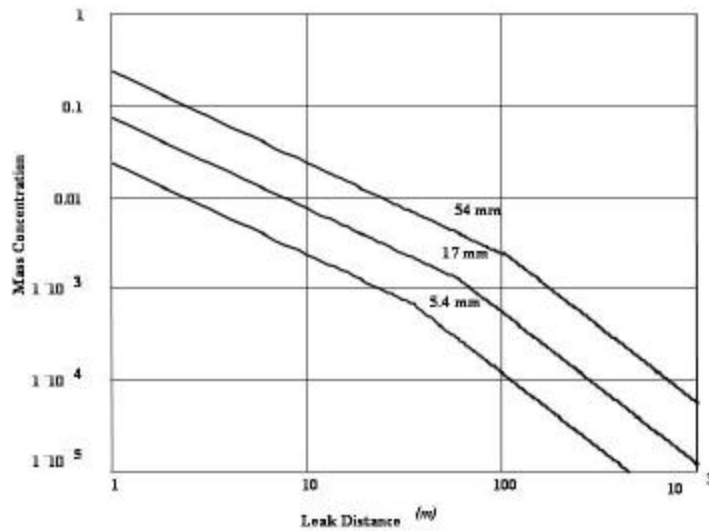


Fig. 3 Methane concentration with distance from the leak.

Radar Scattering Model

The index of refraction of methane is typically higher than that of dry or moist air. Figure 4 gives the resonance shifts of methane compared to dry air for controlled flow tests we performed with a TE_{011} MW cavity. The measured values of permittivity for methane and dry air are 1.000671 and 1.000573, respectively; it is even higher when the cooling effect is considered due to adiabatic expansion of the gas in the jet. From the concentration values of methane, we determined the index of refraction of methane-air mixture and plotted in N units $[(n-1).10^6]$ in Fig. 5(a). When we take into account the

turbulent flow with vortices of a millimeter to a meter scale, the index of refraction fluctuates accordingly. Based on the theory of scattering from the index of refraction fluctuations, the specific volume-scattering cross section is given by⁷

$$\sigma_0 = 2 \cdot \pi \cdot k^4 \cdot \Phi(k), \quad (8)$$

where $\Phi(k)$ is the spectral density of fluctuations of the index of refraction inside the scattering volume and k is the wave number. The spectral density of index of refraction fluctuations according to Kolmogorov's model is given by:⁶

$$\Phi(k) = 0.033 \cdot C_n^2 \cdot k^{-11/6}, \quad \text{for } 2 \cdot \pi / L_0 \leq k \leq 2 \cdot \pi / \ell \quad (9)$$

where C_n is a structural constant characteristic of fluctuations of the index of refraction of the medium, and L_0 and ℓ are vortex sizes of external and internal scales (Fig. 1). The constant C_n is determined from the scale of turbulence and the vertical gradient of the index of refraction.

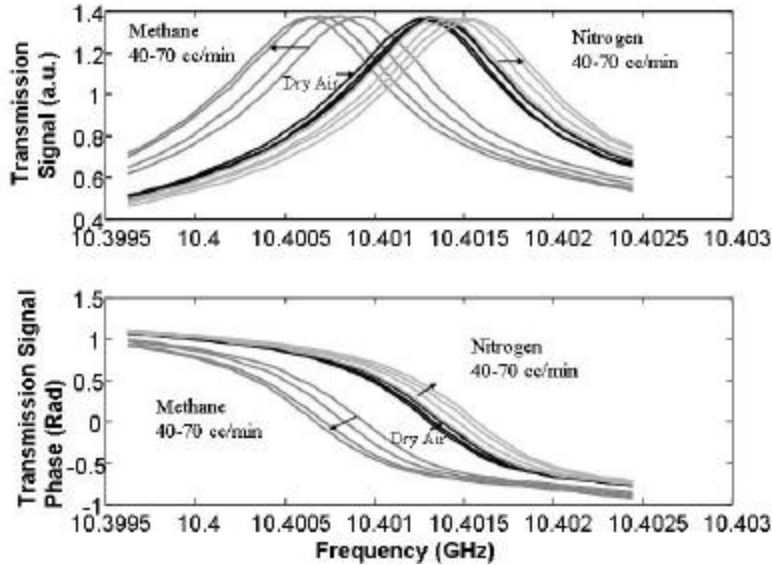


Fig. 4 Resonance shift of microwave cavity signals for methane, nitrogen, and dry air.

Fig. 5 (b) gives the radar reflectivity (or specific volume-scattering cross section) σ_0 of methane plumes for the three leak classes. The corresponding volume-integrated radar cross sections range from 10^{-9} to 10^{-7} m^2 . These values are generally significantly higher in practice because of possible condensation of water vapor from air due to supercooled gases in the jet.

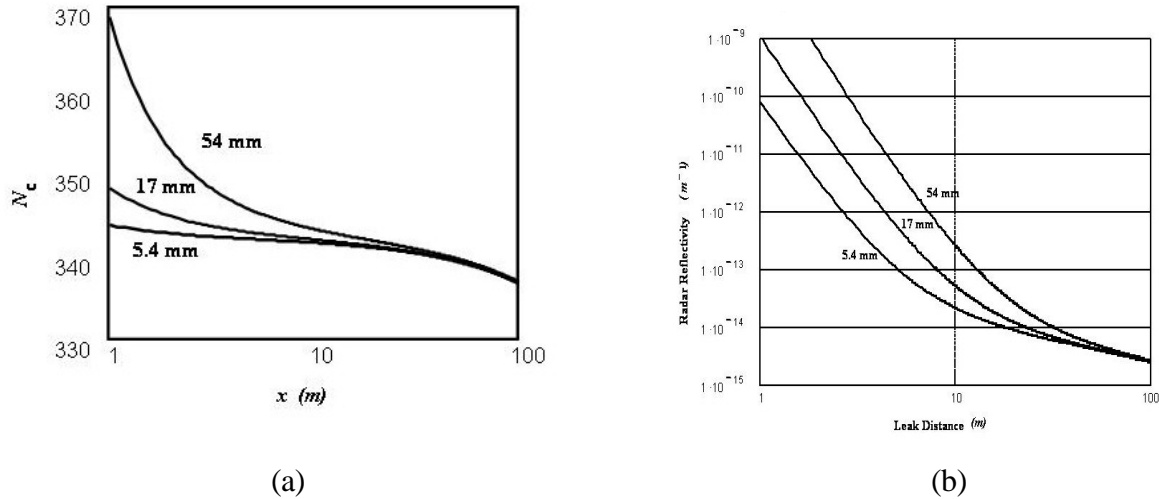


Fig. 5. (a) Index of refraction in N-unit and (b) radar reflectivity of methane plume vs. leak distance.

Equating $P_r = 4 \cdot (\text{receiver noise power})$ in Eq. (1), Figure 6 gives the minimum detectable radar cross section with respect to range of a 6 kW, X band marine radar that we have acquired for model verification and leak testing. Because of the fourth power dependence of the radar signal with range, it shows that the target must be nearer to the transceiver as the cross section of the target gets smaller.⁸ Figure 6 also shows the radar cross sections of methane plumes in comparison with other standard targets. For the chosen radar, the minimum detectable radar cross section curve shows that the methane plume is detectable at near ranges. The distance of detection can be significantly increased by using high-power transmitters, low-noise receivers, and signal averaging. The estimated scattering cross sections of methane leak plumes, although small, are

above the range of normal atmospheric fluctuations of wind, humidity or density, and are detectable by special-purpose radars tuned to volume-scattering targets.

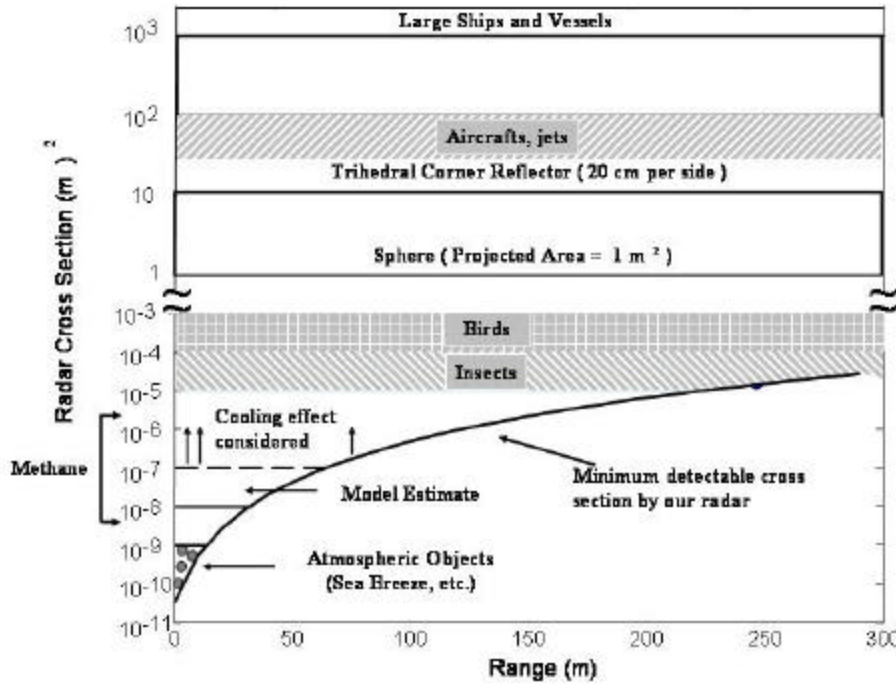


Fig. 6. Radar cross sections of methane plume and other standard targets.

III Radar System Development

To validate the model and to test leak sensitivity, we procured and installed a 6-kW, X-band pulsed imaging radar on the roof of a shed (Fig. 7). Table 1 gives the radar specifications. The antenna, with a slotted waveguide array, provides a vertical beam width of 22° and horizontal beam width of 1.9° . There is a 100- m clearance on one side of the radar setup for leak testing.

Table 1. MARINE RADAR PARAMETERS

1. Peak output power 6 kW

2. Range, Pulse Length and Pulse Repetition Rate (PRR)

Range (km)	Pulse Length (μ s)	PRR (Hz)
0.2315 – 2.778	0.08	2100
2.77 – 5.55	0.3	1200
5.55 – 118.53	0.8	600

3. Minimum Detectable Range 27 m

4. Range Resolution (calculated at minimum detectable range)

In-range 12 m
 Cross-range $0.895 \times 10.36 \text{ m}^2$

5. Range Ring Accuracy (calculated at minimum detectable range) 8 m

6. Antenna Parameters

- Radiator slotted waveguide-array
- Polarization horizontal
- Antenna Rotation 24 RPM
- Radiator Length 120 cm
- Horizontal Beamwidth 1.9°
- Vertical Beamwidth 22°



Fig. 7. Radar set up for near-range leak tests.

The commercial radar was interfaced with a personal computer (PC) for data collection and signal processing. A special purpose Radar Interface Board (RIB) from Xenex was connected to the radar board as a 'slave' device. The RIB was set up as a server and the PC as the client. An Ethernet LAN was used for networking the RIB to the PC. A commercial WinHorizon server software from Xenex ran on the RIB. We modified the client software to control the radar parameters and to perform data recording. We developed our own data processing and display software using Matlab tools. Figure 8 provides the schematic of the hardware setup and the corresponding software modules.

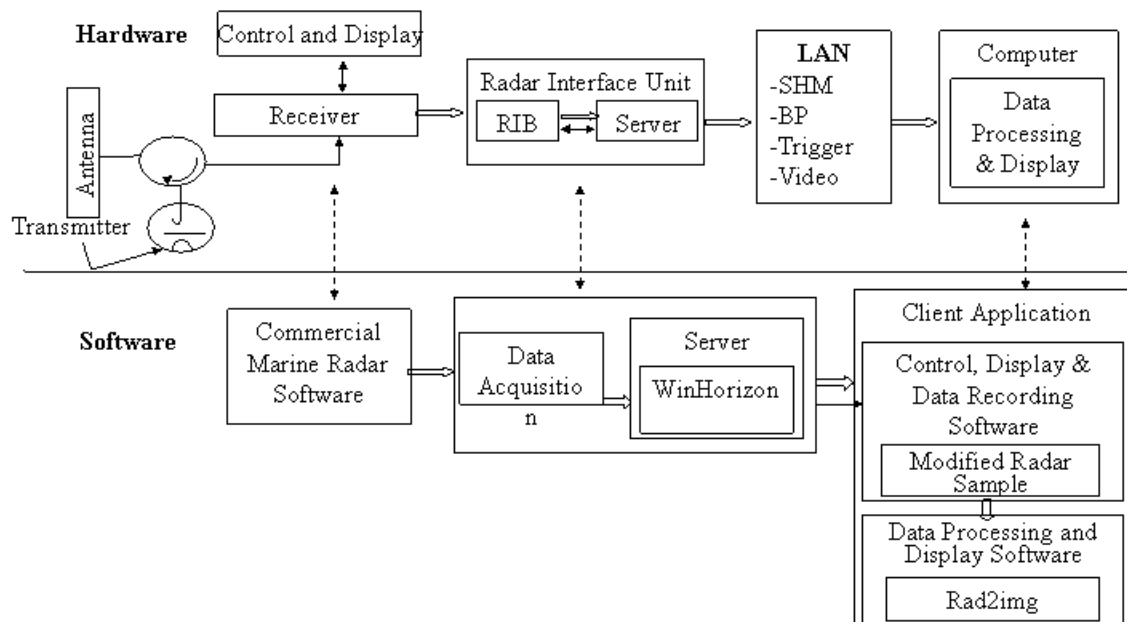


Fig. 8. Schematic of radar data collection.

Radar System Calibration and Modifications

Our first task was to perform the calibration of the radar system. We began by first attempting far field calibration in terms of locating the buildings and structures in the vicinity. We successfully detected and traced the path of an aircraft flying at a high altitude. Next we attempted to detect objects in close ranges. The ground clutter generally overwhelms the target signal at these short ranges. The radar is conveniently located at the edge of a 100 m long clearance. We used a corner cube reflector (each side 20 cm) as a target at 60 m. We needed to use lower receiver gains to bring out the target signal from the clutter. Figure 9 gives the image of the clearance area and of the corner cube at 60 m. The radar cross section of the corner cube, calculated from theory, equals 3.68 m^2 .

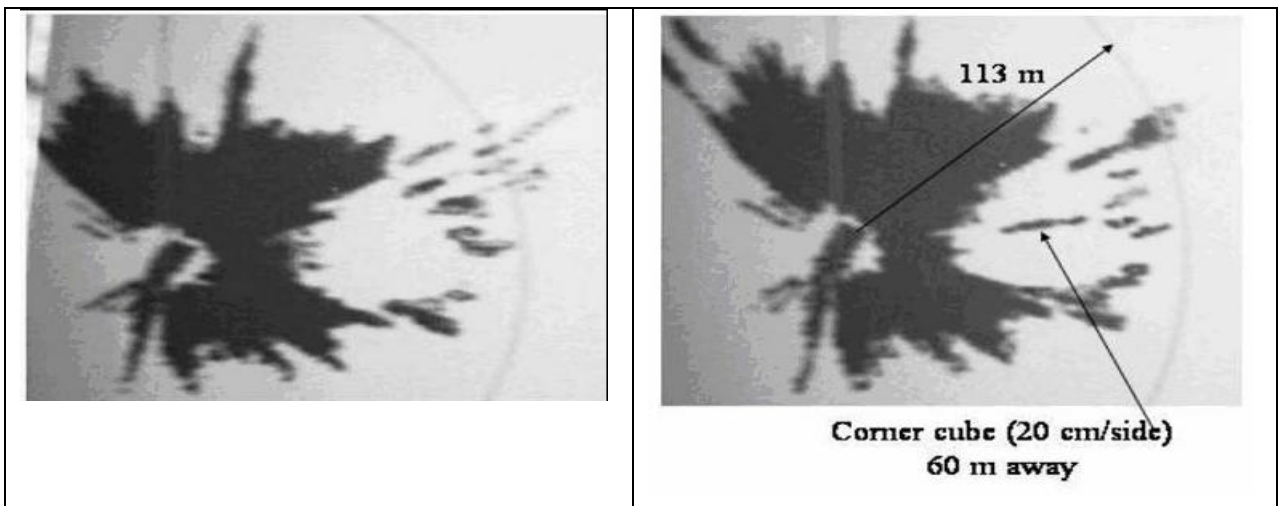


Fig. 9. Radar system calibration with a corner cube.

Initially, the radar was being operated in the normal scanning mode i.e. with the antenna rotating. While this mode is desirable for imaging, it isn't necessarily the optimal mode of operation for initial leak testing. Instead, we operated the radar in the stationary-antenna mode for continuous data collection with signal averaging. Certain modifications had to be made in the radar hardware setup for this purpose. In essence, the radar had to be fooled to believe that the antenna was still rotating by applying the heading marker signal externally from a function generator. Now we could point the

antenna to a specific direction and collect an entire frame of data containing 1024 scan lines corresponding to the same scenario.

Figure 10 show a vector-scope image and a line plot corresponding to the corner cube and a fence located along the radar viewing angle. The echo signals will be in the form of concentric circles in a vector-scope display (Fig. 10a). These scan lines can also be averaged and presented as a line plot of echo signals versus distance (Fig. 10b). We can also animate the line plots as a function of time, which will show the moving targets clearly. The animation of the data showed vividly the rise and fall of the corner cube, when it was tipped during the scan. The animation feature of our software proved very helpful later on in detection of flowing gases.

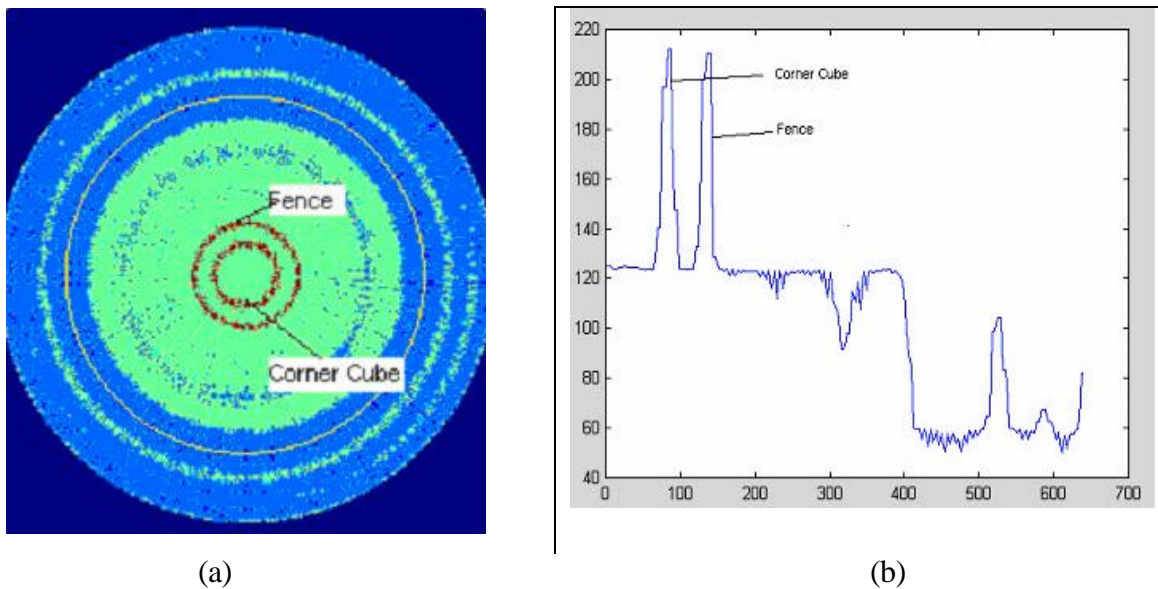
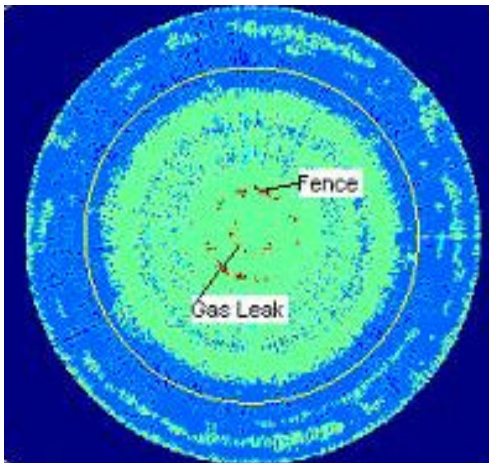


Fig. 10. Detection of corner cube (20cm/side) with a stationary antenna (a) vector-scope image and (b) line plot.

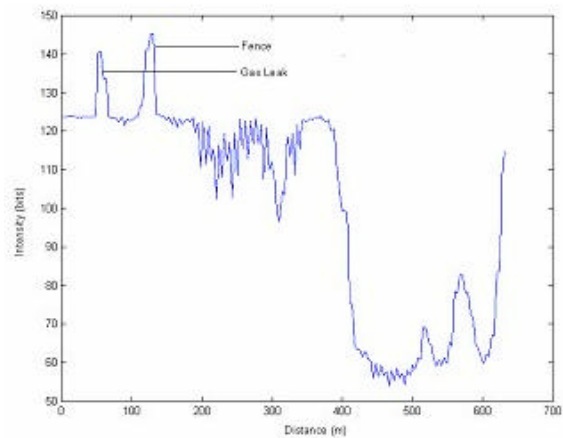
IV Radar Test Results for Gas Plumes

We had done the calibration and testing of our radar system for detecting standard targets at short ranges. To transition from solid reflectors to gas plumes, we first used cold nitrogen plumes from the headspace of a liquid nitrogen dewar. We expected stronger

signals from the cold nitrogen plume because of condensation of water vapor. As described earlier, our leak detection setup faces a 100 meter clearance. Within this clearance, at a distance of 60m from the radar system, we set up a release of cold nitrogen plume from the headspace of a liquid nitrogen dewar. The dewar was kept out of radar sight, and a copper tubing was laid down from the dewar to the point of release where a 2.1-m-high tube section stood up. Beam pointing was achieved with a portable crystal detector. Three sets of data were collected for each experiment, i.e., before, during, and after the gas release. Figures 11 and 12 show the results from one such experiment. There was a clear difference between the reflected signals, with and without the gas flowing. The enhanced radar return is a result of water vapor condensation in the plume area.



(a)



(b)

Fig. 11. Detection of cold nitrogen plume with a stationary antenna (a) vector-scope image and (b) line plot.

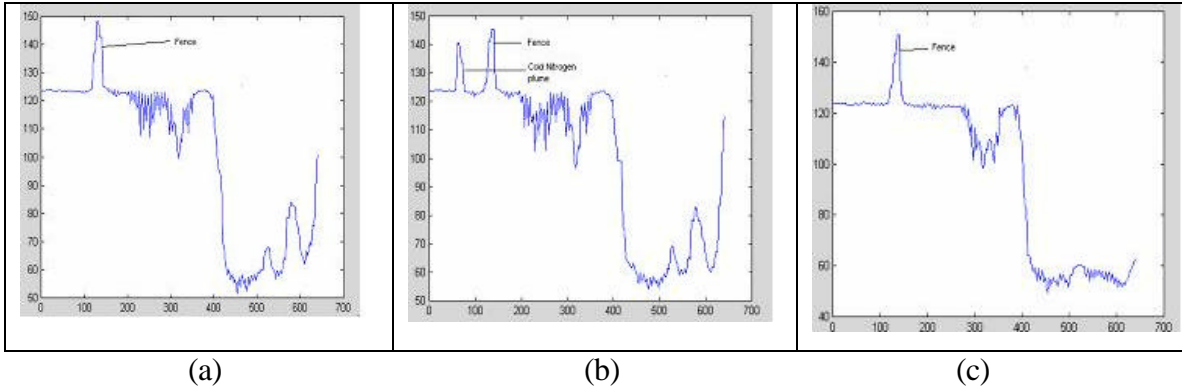


Fig. 12. Cold Nitrogen plume detection scenario (a) before the release, (b) during the release; and (c) after the release.

With a subcontract from Argonne, our collaborator, AOZT FINN-TRADE of St. Petersburg, Russia used similar radar and conducted propane gas releases in a suburb of St. Petersburg. As is depicted in Fig. 13, the leak was setup in a zone of radar shade from a land relief, which minimizes the influence of ground objects. The experiment was carried out in calm weather conditions (ambient air temperature 19°C, pressure 100.8 kPa, humidity 87%, and wind speed 0 to 0.2 m/s).

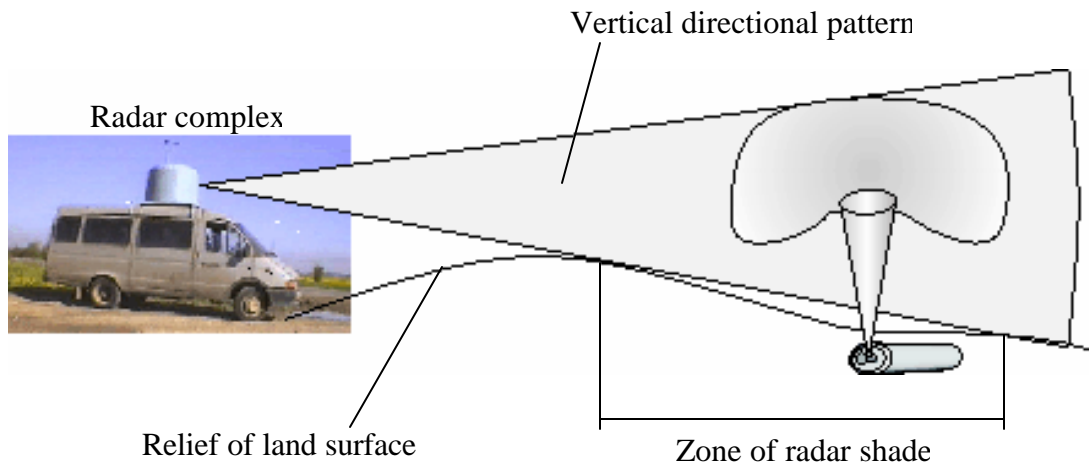


Fig. 13. Scheme of gas ejection sounding in the zone of radar shade.

The location of the experiment was a secluded dirt road in the country side with almost

no vehicular traffic. First a corner cube was placed at the intended location of gas release and the corresponding data collected. The gas leak was set up by opening the valve of a 50-liter cylinder at a rate of 7.5 g/s. The cylinder contained a mixture of Propane and Butane gases. Data were recorded during the gas release at two distance channels corresponding to gas location and the background. The signal corresponding to the gas release was in the 12th distance channel (720 m) and that of the background was in the 18th channel (990 m). Figure 14 shows the comparison of the return signals for gas and background.

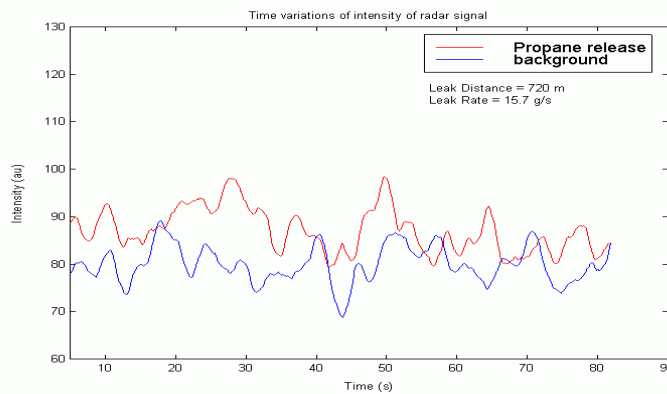


Fig. 14. Radar detection of propane leak 720 m away.

The radar cross section, when calculated with reference to the corner cube, came to $2.6 \cdot 10^{-7}$ to $3.0 \cdot 10^{-7} \text{ m}^2$. The model prediction of propane plume from a 50-l cylinder at a pressure of 8.5 kgf/cm^2 with a leak diameter of 4 mm is $1.3 \cdot 10^{-7} \text{ m}^2$, which is in good agreement with the experimental value.

Investigation of radar detection at millimeter-wave frequencies

The specific radar cross-section of a gas plume generally increases with frequency; the range of applicable frequencies is determined by the vortex sizes of the turbulent flow. Based on Eqs. 8 - 9, the specific radar cross section increases with frequency as shown in Fig. 15. In order to test the dependence of radar returns with frequency, we conducted experiments with a 94-GHz millimeter-wave radar (Fig. 16a). It is a low-power (100

mW) continuous-wave radar with a lens antenna for near-field focusing. The millimeter wave radar was pointed at steam coming out from a valve in a high pressure steam pipeline at a distance of 10 meters. Figures 16b shows the millimeter-wave reflected signals collected from the steam plume and the background winter-time air. Even though the transmitted power is in low, an observable radar return was obtained due to the following confluent factors: condensation effect of steam in cold air, short range of detection, and lower wavelength. A pulsed high-power millimeter-wave radar, therefore, is expected to provide higher sensitivity of detection for gas leaks.

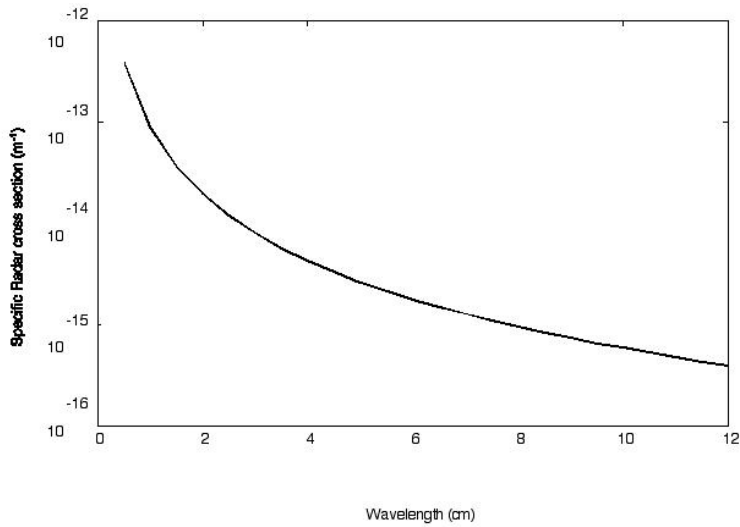
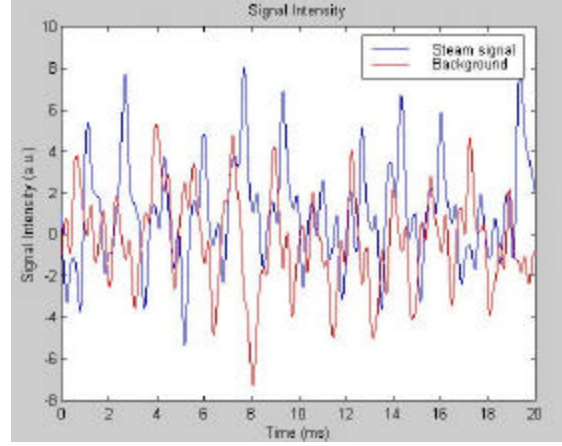


Fig. 15. Change of specific radar cross section with wavelength.



(a)



(b)

Fig. 16. Millimeter wave leak detection (a) Hardware setup; (b) comparison of steam and background (no steam).

V Conclusion

Modeling of radar cross section is an essential step in assessing the feasibility of radar technique for detection of weak targets such as gas plumes. We modeled the leak plumes emanating from small holes in a pressurized gas pipeline. With a gas dynamic model, we determined the geometry of plume dispersion in the atmosphere and the variation of methane concentration in the air surrounding the leak. For a typical gas line, a leak from a hole of a few millimeters is a turbulent jet in the shape of a cone. A fairly large size plume is possible; the plume diameter at a distance of 100 m from a 5.4 mm leak, for example is, is 44 m and the corresponding methane concentration is 100 ppm. A knowledge of the plume geometry is useful to determine the required resolution of the radar.

From the concentration changes of methane-air mixture in the plume geometry, we determined the static and dynamic changes in the index of refraction. With a scattering model based on the inhomogeneities of the index of refraction, the radar cross section of the plume was calculated. An estimate of 10^{-9} to 10^{-7} m² was predicted for radar cross section of leaks emanating from a 5.4-mm to 54-mm diameter hole. The estimated range of radar cross section lies above the normal fluctuations of the atmosphere and is well

within the detectable range of special-purpose radars. Much higher cross section than predicted by the model is possible in practice if we take into account the cooling effect of an expanding jet and the attendant water vapor condensation.

Based on an X band marine radar, we built a computer-interfaced radar system to process the weak signals that are expected from gas plumes. The system can operate either in imaging mode in which the antenna scans and collects plan-position images or in a staring mode in which the antenna is stationary and pointed to the plume and collects reflected signals as a function of distance. The processing of signals and images such as filtering and averaging is performed with Matlab software tools. After calibrating the radar with a corner cube of known cross section, we tested the radar returns from several solid structures including buildings and fence line near the radar setup.

Two gas plume tests were conducted, one with a cold nitrogen plume at 60 m from a liquid nitrogen dewar for initial testing and the other a propane leak from a 50-l cylinder at 720 m from the radar. Because of condensation, the cold nitrogen plume was easily detected even for small leaks. The propane leak test was more realistic in that it simulated the spread and dynamics of a methane leak as well as its radar cross section closely, and it was safe and environmentally permissible for release. The radar signals obtained between two distance channels corresponding to the plume and background atmosphere showed clear change in signal level for propane plume. The radar cross section of the propane plume, calculated from the radar return, agreed with the model results to a close approximation.

In summary, we make the following conclusions.

The theoretical and experimental results show feasibility of the radar technique for remote detection and imaging of above-ground gas pipeline leaks. The technique has the potential to detect below-ground pipeline leaks also because of the expected enhancement of the radar cross section of the leaking gas entrained with the soil moisture and dust.

With a special purpose radar of high-power transmitter, high-gain-low-noise receiver, and an image processing software tailored to gas plume detection, remote and fast inspection of thousands of miles of above- and below-ground pipelines in a flyby mode is feasible.

Reference:

1. U.S. DOE/NETL report, "Natural gas infrastructure reliability: pathways for enhanced integrity, reliability, and deliverability," DOE/NETL-2000/1130, 2000.
2. R. J. Doviak and D. S. Zrnic, *Doppler Radar and Weather Observations*, Academic Press, New York, 1984.
3. N. Gopalsami and A. C. Raptis, "Microwave radar sensing of gas pipeline leaks: A state of the art of the technology," Report to DOE-NETL, Dec. 2001.
4. M. Skolnik (ed.), *Radar Handbook*, New York: McGraw-Hill, 1990.
5. M. Skolnik, D. Hemenway, and J. P. Hansen, "Radar Detection of Gas Seepage Associated with Oil and Gas Deposits," *IEEE Trans. on Geoscience and Remote Sensing*, vol. 30, pp. 630-633, 1992.
6. G. N. Abramovich, *The Applied Gas Dynamics*, Moscow: Nauka, 1969.
7. A. Ishimaru, *Wave Propagation and Scattering in Random Media*, vol. 2, New York: AP, 1978.
8. N. Gopalsami, D. B. Kanerykin, V. D. Asanov, S. Bakhtiari, and A. C. Raptis, "Microwave radar detection of gas pipeline leaks," *Review of Quantitative Nondestructive Evaluation*, ed. D. O. Thompson and D. E. Chimenti, American Institute of Physics, vol. 22, pp. 478-484, 2003.